



Lead citrate precursor route to synthesize nanostructural lead oxide from spent lead acid battery paste

Lei Li^a, Yuchen Hu^a, Xinfeng Zhu^{a,b}, Danni Yang^a, Qin Wang^a, Jianwen Liu^a, R. Vasant Kumar^c, Jiakuan Yang^{a,*}

^a School of Environmental Science and Engineering, Huazhong University of Science and Technology (HUST), 1037 Luoyu Road, Wuhan, Hubei 430074, PR China

^b Henan University of Urban Construction, Pingdingshan, Henan 467000, PR China

^c Department of Materials Science and Metallurgy, University of Cambridge, Cambridge CB2 3QZ, UK

ARTICLE INFO

Article history:

Received 22 November 2012

Received in revised form 28 December 2012

Accepted 7 January 2013

Available online 23 January 2013

Keywords:

A. Nanostructures

B. Chemical synthesis

C. Thermogravimetric analysis

C. X-ray diffraction

D. Electrochemical properties

ABSTRACT

Nanostructural lead oxides were prepared by the decomposition of a new type of lead citrate precursor ($\text{Pb}_3(\text{C}_6\text{H}_5\text{O}_7)_2 \cdot 3\text{H}_2\text{O}$), which was synthesized through leaching of spent lead acid battery paste in citrate salt aqueous system and more economical compared with former precursor ($\text{Pb}(\text{C}_6\text{H}_6\text{O}_7) \cdot \text{H}_2\text{O}$). The products were characterized by thermogravimetric–differential thermal analysis, scanning electron microscopy and X-ray diffraction. The results show that when lead citrate of columnar-shape crystals are calcined in N_2 gas, orthorhombic β -PbO is the main product containing small amount of Pb and C. On combusting the citrate in air, a mixture of orthorhombic β -PbO, tetragonal α -PbO and Pb with the particle size of 100–200 nm is obtained, with β -PbO as the major product. And the cyclic voltammetry measurements of lead oxides present different electrochemical redox potentials because of the different structure of lead oxide obtained from $\text{Pb}_3(\text{C}_6\text{H}_5\text{O}_7)_2 \cdot 3\text{H}_2\text{O}$.

Crown Copyright © 2013 Published by Elsevier Ltd. All rights reserved.

1. Introduction

Recently, the synthesis of nanostructural oxide materials has attracted considerable attention of chemists and metallurgists [1–3]. Lead oxide has many crystalline forms, such as PbO (α , β), Pb_2O_3 , Pb_3O_4 , and PbO_2 (α , β). Lead dioxide (PbO_2), which is used as a positive active material in lead acid battery, has been extensively studied. In lead acid batteries, PbO is the starting paste material for both anode and cathode, which is then converted to active Pb and PbO_2 during cell formation stage. There is a big interest to improve lead oxide characteristics to obtain more discharge capacity and long cycle-life. It is expected that the lead oxide in form of nano-particulates can deliver more electrical energy at discharge process due to its large specific surface area and good reversible property. Wang et al. [3] prepared nano crystalline lead oxide through two-step chemical reactions. Salavati-Niasari et al. [4] reported that synthesis of nano-size lead oxide powder with an average particle size of 35 nm could be made by decomposing lead oxalate at 500 °C. Sadeghzadeh et al. [5] used 2-pyridinecarboxylic acid, lead acetate and sodium nitrite to synthesize one-dimensional structure of Pb (II) chelate, which

was roasted at 110–500 °C, to produce PbO nanostructures. The research results from Cruz et al. [6] showed that α -PbO thin films were prepared by spray pyrolysis of aqueous solutions of $\text{Pb}(\text{CH}_3\text{COO})_2 \cdot 3\text{H}_2\text{O}$ and deposited onto a lead substrate. The battery cell maintained a discharge capacity of 100 mAh g^{-1} of positive plate (40 wt% of the theoretical value) upon extensive cycling. Karami et al. [7,8] synthesized a uniform nano-structured lead oxide via sonochemical method. The electrochemical tests showed that a large discharge capacity and excellent cycle characteristics of the nanostructural powder were obtained.

In previous study, the synthesis process of nano-structured lead oxide is more or less complex because of the utilization of sonochemical technology. And the starting materials are lead compounds, such as $\text{Pb}(\text{NO}_3)_2$, $\text{Pb}(\text{CH}_3\text{COO})_2 \cdot 3\text{H}_2\text{O}$, which are expensive as pure chemical reagents. Citrate precursor route has been used in the preparation of nano-structured materials widely [9–11]. This route contains two steps: one is the synthesis of citrate precursors, and the second is the decomposition of citrate precursors. And different structured precursors can obtain different nano-structured materials. However, there is little report about synthesis of nanostructural lead oxide using citrate precursor route. The lead citrate precursor can be readily converted to PbO (containing some Pb) for directly making lead acid battery pastes with controllable degree of metallization by a combustion–calcination process [12–14].

* Corresponding author. Tel.: +86 27 87792207; fax: +86 27 87792101.

E-mail addresses: jkyang@mail.hust.edu.cn, yjiakuan@hotmail.com (J. Yang).

In our previous research [15], the lead citrate ($\text{Pb}(\text{C}_6\text{H}_6\text{O}_7)\cdot\text{H}_2\text{O}$) was synthesized from spent lead acid battery pastes in citric acid system, and nano lead oxide with particle size of 100–200 nm was obtained from calcination–combustion. The precursor, with formula of $\text{Pb}(\text{C}_6\text{H}_6\text{O}_7)\cdot\text{H}_2\text{O}$, was generated in the 3–4 pH range in citric acid system. Due to the various types of citrate ions ($\text{C}_6\text{H}_7\text{O}_7^-$, $\text{C}_6\text{H}_6\text{O}_7^{2-}$ and $\text{C}_6\text{H}_5\text{O}_7^{3-}$) and lead's effective interactions with organic molecules, some other Pb-citrate types, such as $\text{Pb}_3(\text{C}_6\text{H}_5\text{O}_7)_2\cdot 3\text{H}_2\text{O}$, can be synthesized in this citric acid system by changing the reaction conditions. Unlike the former lead citrate ($\text{Pb}(\text{C}_6\text{H}_6\text{O}_7)\cdot\text{H}_2\text{O}$), $\text{Pb}_3(\text{C}_6\text{H}_5\text{O}_7)_2\cdot 3\text{H}_2\text{O}$ has a different morphology and its crystals particle can grow up to some extent, which could improve filtration performance of lead citrate. Moreover, the ratio of lead to citrate of $\text{Pb}(\text{C}_6\text{H}_6\text{O}_7)\cdot\text{H}_2\text{O}$ is 1:1, whereas the ratio of that in $\text{Pb}_3(\text{C}_6\text{H}_5\text{O}_7)_2\cdot 3\text{H}_2\text{O}$ is 3:2. It is indicated that the consumption of citrate ions in the synthesis of $\text{Pb}_3(\text{C}_6\text{H}_5\text{O}_7)_2\cdot 3\text{H}_2\text{O}$ with per mol Pb^{2+} is less than the consumption in the synthesis of $\text{Pb}(\text{C}_6\text{H}_6\text{O}_7)\cdot\text{H}_2\text{O}$. Even though $\text{Pb}_3(\text{C}_6\text{H}_5\text{O}_7)_2\cdot 3\text{H}_2\text{O}$ is of advantages in the lead citrate precursor route to synthesize nanostructural lead oxide, there is a lack of knowledge about the decomposition process of $\text{Pb}_3(\text{C}_6\text{H}_5\text{O}_7)_2\cdot 3\text{H}_2\text{O}$ and the characteristics of decomposition products. In this work, as shown in Fig. 1, the nanostructural lead oxide was prepared via a low temperature calcination process both in N_2 gas and air, by using a new lead citrate type ($\text{Pb}_3(\text{C}_6\text{H}_5\text{O}_7)_2\cdot 3\text{H}_2\text{O}$) as a precursor. The decomposition process and the characteristics of nanostructural lead oxide have been discussed in detail. By controlling the calcination process of lead citrate, it is possible to obtain variation in the microstructure from nano to micro scale, and nano-powders are attractive for future development work in advanced lead acid batteries.

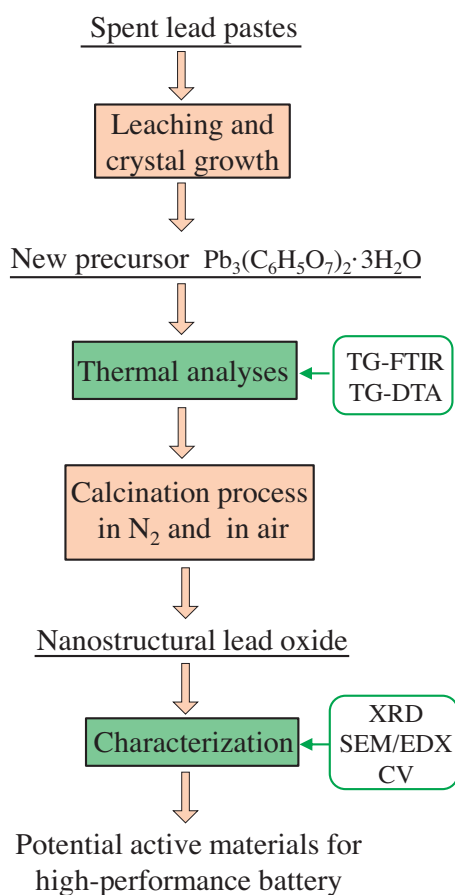


Fig. 1. The procedure of preparing nanostructural lead oxide by the decomposition of a new lead citrate precursor ($\text{Pb}_3(\text{C}_6\text{H}_5\text{O}_7)_2\cdot 3\text{H}_2\text{O}$).

Table 1

Chemical composition of spent lead acid battery paste.

Constituent Percentage (%)	PbSO ₄	PbO ₂	PbO	Pb	Others
	56.8	32.4	4.2	5.5	1.1

2. Experimental

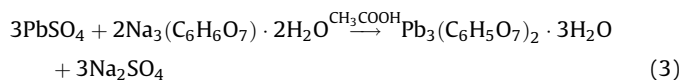
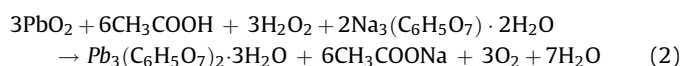
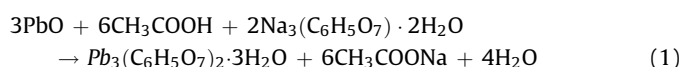
2.1. Materials

The samples of spent lead acid battery pastes were provided by Hubei Jinyang Metallurgical Co. Ltd., China, where the waste lead pastes are treated to recover lead metal using a conventional smelting process. The chemical composition of the spent lead acid battery pastes is shown in Table 1.

Trisodium citrate hydrate ($\text{Na}_3\text{C}_6\text{H}_5\text{O}_7\cdot 2\text{H}_2\text{O}$, >99% purity) was used as the desulfating agent and organic ligand during leaching spent lead battery pastes. Anhydrous acetic acid (CH_3COOH , 99.5% purity) was used to leaching and keeping balance of pH. Hydrogen peroxide (H_2O_2 , 30%, w/v) was used as the reductant.

2.2. Synthesis of lead citrate precursor

The reaction in this leaching system can be represented by the following equations [(1)–(3)].



In this leaching experiment, 10 g of spent lead battery paste was added to trisodium citrate and anhydrous acetic acid and 30% peroxide hydrogen solution with a solid/liquid mass ratio of 1/5. The calculated and actual dosages of each leaching reagents are shown in Table 2. In order to transform all lead compounds in spent lead battery paste into lead citrate, the actual dosage of $\text{Na}_3\text{C}_6\text{H}_5\text{O}_7\cdot 2\text{H}_2\text{O}$ was 14.4 g and CH_3COOH was 6.6 g, which were both twice of calculated dosage. The actual dosage of H_2O_2 was 5.6 mL (a quadruple calculated dosage). The pH of the solution was in a range of 5–6. Leaching was carried out under magnetic stirring at speed of 650 rpm to maintain full suspension of the slurry for 5 h at room temperature (25 °C). During leaching, lead citrate began to crystallize from the solution at the room temperature. After leaching, the reaction vessel with lead citrate slurry was left in homoeothermic water bath at 55 °C for 8 h. The lead citrate crystals grown up, then the resulting crystals were washed with distilled water; vacuum filtrated and dried at 45 °C. The concentration of lead ion in the left solution was analyzed with atomic absorption spectrometry (WFX-100, Beifen-Ruili, China).

2.3. Thermal analyses of lead citrate

Thermal analyses of the lead citrate were performed in corundum crucible by thermogravimetric–differential thermal

Table 2

The calculated and actual dosages of each leaching reagents.

Leaching reagents	$\text{Na}_3\text{C}_6\text{H}_5\text{O}_7\cdot 2\text{H}_2\text{O}$ (g)	CH_3COOH (g)	H_2O_2 (30%) (mL)
Calculated dosages	7.2	3.3	1.4
Actual dosages	14.4	6.6	5.6

analysis (TG–DTA), in different atmospheres using TA Instruments (Diamond TG–DTA, Platinum–Selmer Equipment Co. Ltd., Shanghai), with air or nitrogen gas under a flow rate of $100 \text{ cm}^3 \text{ min}^{-1}$ by heating up to $800 \text{ }^\circ\text{C}$ at heating rate of $5 \text{ }^\circ\text{C min}^{-1}$. Thermogravimetric–Fourier Transform Infrared Spectroscopy (TG–FTIR) was used to analyze the tail gas. When the tail gas was generated during decomposition of lead citrate in the thermogravimetric instrument, it was sent directly to the connected Fourier Transform Infrared Spectroscopy instrument to analyze. The experiment was carried out by using TA Instrument (STA 409, NETZSCH Scientific Instrument Co. Ltd., Germany) and FTIR Instrument (EQUINOX 55, Bruker corporation, Germany), both in air and nitrogen gas under a flow rate of $79 \text{ cm}^3 \text{ min}^{-1}$ by heating up to $600 \text{ }^\circ\text{C}$ at heating rate of $5 \text{ }^\circ\text{C min}^{-1}$.

2.4. Calcination of lead citrate

The calcination behaviors of lead citrate were investigated in a tubular atmosphere furnace in different atmospheres. In nitrogen gas, the lead citrate powders of 2 g were calcined at $295 \text{ }^\circ\text{C}$, $335 \text{ }^\circ\text{C}$, $350 \text{ }^\circ\text{C}$, $400 \text{ }^\circ\text{C}$ and $450 \text{ }^\circ\text{C}$ for 2 h, respectively, at heating rate of $10 \text{ }^\circ\text{C min}^{-1}$. In the air, the citrate powders of 2 g were calcined at $120 \text{ }^\circ\text{C}$, $300 \text{ }^\circ\text{C}$, $350 \text{ }^\circ\text{C}$, $370 \text{ }^\circ\text{C}$, $415 \text{ }^\circ\text{C}$, $450 \text{ }^\circ\text{C}$ and $550 \text{ }^\circ\text{C}$ for 1 h, respectively. The lead citrate powders of 2 g were also calcined isothermally at $350 \text{ }^\circ\text{C}$ with variation of time, such as 5 min, 10 min, 15 min, 20 min, 40 min and 60 min in air. The weight loss was measured for each set of the experiments. Calcination temperature was determined based on TG–DTA data.

2.5. Characterization of materials

X-ray diffraction (XRD) data were collected from powder samples using a X'Pert PRO XRD (Philips, PAN alytical B.V., Holland) with $\text{Cu K}\alpha$ radiation and $\lambda = 1.5418 \text{ \AA}$ at scanning rate of 0.28° per second for 2θ in the range from 5° to 75° . In order to identify new lead citrate precursor, $\text{Pb}_3(\text{C}_6\text{H}_5\text{O}_7)_2 \cdot 3\text{H}_2\text{O}$ purchased from Alfa Aesar China (Tianjin) Co., Ltd. (CAS number: 6107-83-1) was used as the reference in XRD analysis. Morphology studies were carried out with scanning electron microscopy (Sirion 200SEM, FEI, Holland) operated at 10 kV after coating the samples with gold. EDX spectra of the calcined products were collected on an ultra-thin window (UTW) X-ray detector equipped with Sirion 200 SEM.

2.6. Characterization of lead oxide with electrochemical measurements

Cyclic voltammetry (CV) was employed to investigate the electrochemical behavior of the lead oxide. The CV curves were determined with a typical three-electrode system. The working electrode (WE) was prepared from platinum microelectrode which was filled with lead oxide. PbO in contact with concentrated sulfuric acid was converted into PbSO_4 which then acted as the electrochemically active precursor in the electrode for formation of PbO_2 via oxidation. A double platinum electrode was used as the counter electrode while $\text{Hg}/\text{Hg}_2\text{SO}_4/\text{K}_2\text{SO}_4$ (sat.) was employed as the reference electrode. Sulfuric acid solution at concentration of 3 mol L^{-1} was used as electrolyte. CV was performed for 7 cycles at room temperature ($22 \text{ }^\circ\text{C}$) using electrochemical workstation (VMP-2, Princeton, USA), with a scanning speed of 20 mV s^{-1} in a potential range of 0 V to +1.5 V.

3. Results and discussion

3.1. Crystallization of lead citrate

After leaching, the spent solution was diluted in the 1000 mL volumetric flask. Recovery of lead was calculated by subtracting

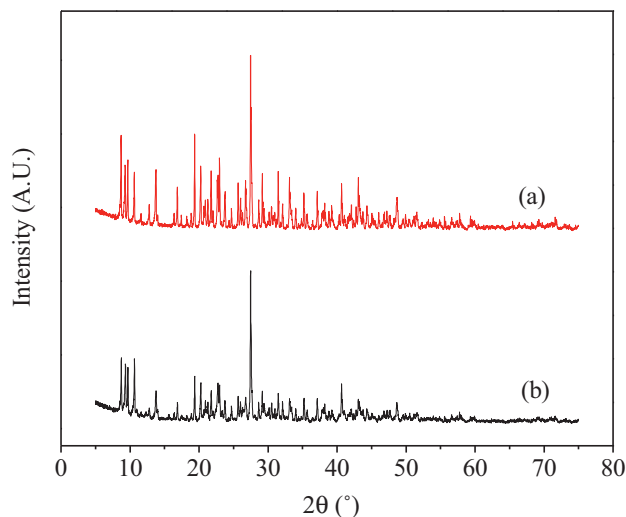


Fig. 2. XRD patterns of (a) crystals obtained from spent lead acid battery pastes and (b) lead citrate $\text{Pb}_3(\text{C}_6\text{H}_5\text{O}_7)_2 \cdot 3\text{H}_2\text{O}$ from Alfa Aesar China (Tianjin) Co., Ltd. (CAS: 6107-83-1).

the mass of lead in the spent solution, which was to be 96.0 wt%. The XRD pattern of the resulting crystals are shown in Fig. 2, compared with the XRD pattern of lead citrate. None of the original lead phases are observed in the XRD patterns (a), indicating that the reaction undergone completely. The pattern of XRD almost matches with lead citrate structural data of $\text{Pb}_3(\text{C}_6\text{H}_5\text{O}_7)_2 \cdot 3\text{H}_2\text{O}$ which was purchased from Alfa Aesar China (Tianjin) Co., Ltd. (CAS number: 6107-83-1). Thus, it can be indicated that the leaching product is $\text{Pb}_3(\text{C}_6\text{H}_5\text{O}_7)_2 \cdot 3\text{H}_2\text{O}$. The photograph of the lead citrate product is shown in Fig. 3(a). Lead citrate precursor is white, which is different from the brown color of spent lead acid battery paste samples. Morphology of the lead citrate is shown in Fig. 3(b). The lead citrate is columnar shaped with length of $5\text{--}50 \text{ }\mu\text{m}$ and diameter of $2\text{--}50 \text{ }\mu\text{m}$. These crystals are easy to filter out of the leaching solution.

3.2. Thermal analyses results

Thermal decomposition of lead citrate was identified with thermal analysis. The TG–DTA curves of the lead citrate in two different atmospheres are shown in Fig. 4. In the pure nitrogen atmosphere, decomposition of the citrate is supposed to take place through pyrolysis. From patterns (a), when the temperature is in the range of $20\text{--}350 \text{ }^\circ\text{C}$, there are three obvious stages of weight loss in the TG curve in N_2 , which corresponds to endothermic peaks in the DTA curve. The mass loss at $200 \text{ }^\circ\text{C}$ is approximately 5.3% that is most likely due to dehydration. Then lead citrate decomposes at $295 \text{ }^\circ\text{C}$ and $335 \text{ }^\circ\text{C}$, respectively. It has been reported that [16] PbO could be reduced to Pb metal by carbon above $370 \text{ }^\circ\text{C}$ in N_2 gas. As shown in Fig. 4(a), the mass loss keeps increasing slowly when temperature rises from $350 \text{ }^\circ\text{C}$ to $800 \text{ }^\circ\text{C}$. This may be reasoned from the reduction of PbO by carbon. It shows that thermal decomposition of $\text{Pb}_3(\text{C}_6\text{H}_5\text{O}_7)_2 \cdot 3\text{H}_2\text{O}$ in N_2 can be completed around and above $350 \text{ }^\circ\text{C}$ with a total weight loss about 32 wt%. Therefore, the temperature for decomposing lead citrate in nitrogen can be selected progressively near the three stages of weight loss, i.e. $295 \text{ }^\circ\text{C}$, $335 \text{ }^\circ\text{C}$, $350 \text{ }^\circ\text{C}$ and $400 \text{ }^\circ\text{C}$, $450 \text{ }^\circ\text{C}$. The FTIR spectrums of tail gas generated during the pyrolysis of lead citrate in N_2 are shown in Fig. 5(a). The absorption in the spectral range of $2400\text{--}2250 \text{ cm}^{-1}$ and $3950\text{--}3500 \text{ cm}^{-1}$ shows that CO_2 and H_2O are the main gas products in the temperature range of $250\text{--}400 \text{ }^\circ\text{C}$.

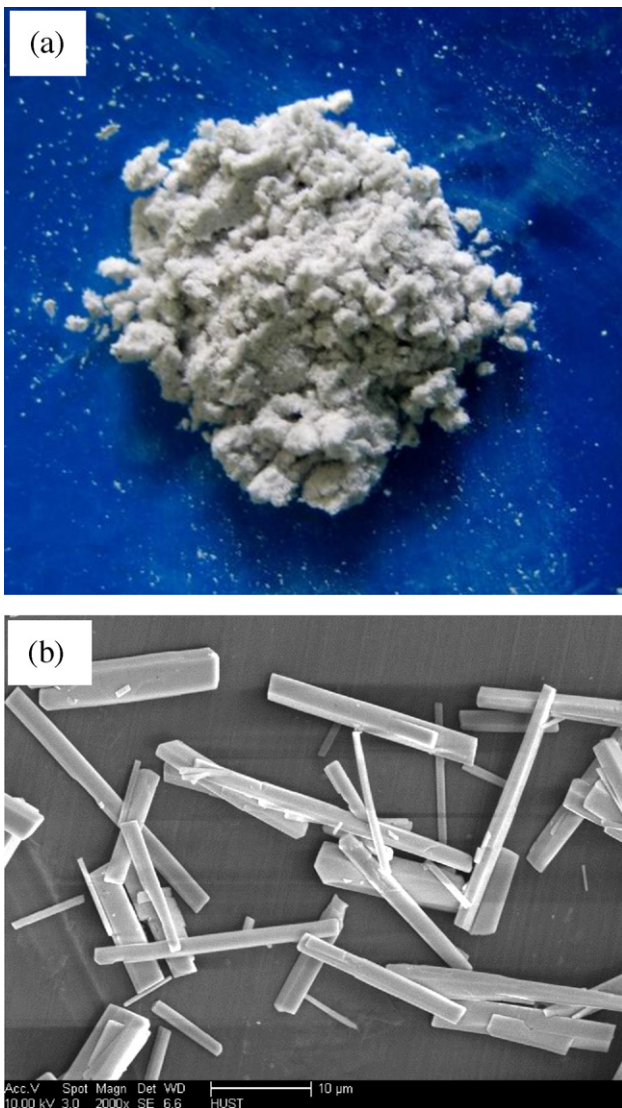


Fig. 3. Photograph and SEM image of lead citrate product: (a) photograph of lead citrate after filtering and (b) SEM image.

Thermal analysis patterns (b) show that the thermal behavior is more complex in air. The first stage of weight loss in 200 °C is due to dehydration. In the following stages, weight loss takes place in the temperature range 270–450 °C, which is ascribed to combustion of the citrate. This process is accompanied by four somewhat overlapping exothermic peaks in DTA curve around 300 °C, 345 °C, 370 °C and 415 °C. Exothermic peaks observed in the DTA curve are ascribed to the oxidation of both C and H from the citrate. When temperature is above 450 °C, both weight loss and heat flow remain constant up to 800 °C. The calcination–combustion temperatures for the citrate can be selected progressively corresponding to the exothermic peaks, at 120 °C (for confirming dehydration reaction in the decomposition process), 300 °C, 350 °C, 370 °C, 415 °C, 450 °C and 550 °C. The FTIR spectrums of tail gas are shown in Fig. 5(b). As the same in N₂, CO₂ and H₂O are the main gas products during the decomposition of lead citrate in the range of 250–400 °C.

According to Fig. 4, when temperature is under 350 °C, the TG curve in air is similar to TG in N₂, and the peak temperatures of DTA curve in air is identical to the results in N₂. When temperature is in range of 350–450 °C, the TG curve in air shows a slope, while TG curve in N₂ is an approximately flat line. It can be inferred that

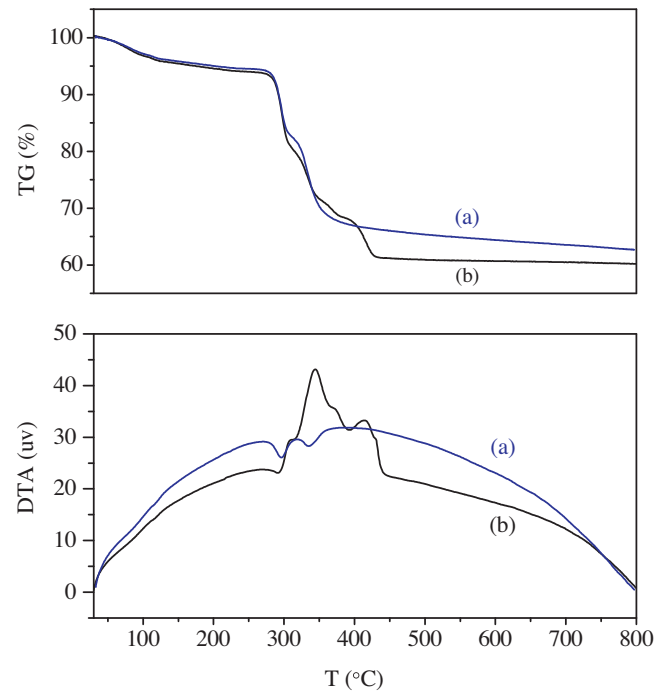


Fig. 4. TG-DTA curves of lead citrate in different atmospheres: (a) in nitrogen gas and (b) in air.

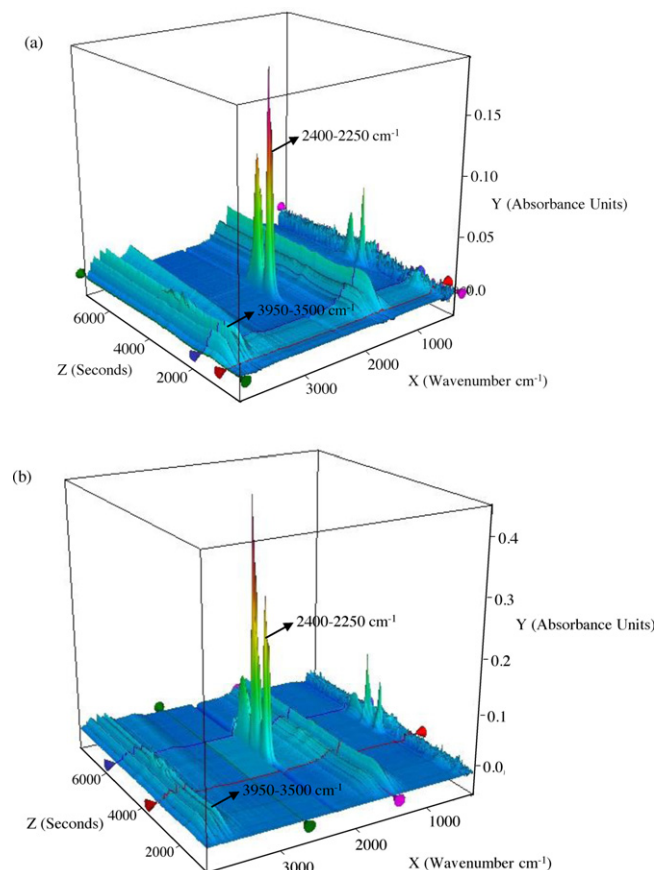


Fig. 5. FTIR spectrums of tail gas generated during decomposition of lead citrate in different atmospheres: (a) in nitrogen gas and (b) in air.

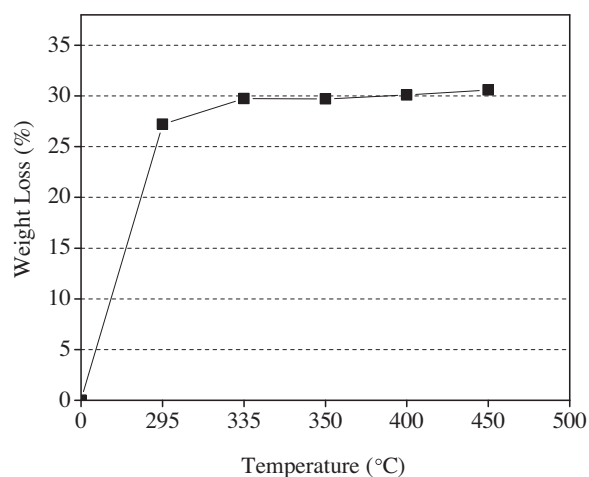


Fig. 6. Effects of calcination temperatures on weight loss of lead citrate in N_2 .

there are two stages taking place in the calcination of $Pb_3(C_6H_5O_7)_2 \cdot 3H_2O$ in air. One stage is decomposition of citrate which is alike of pyrolysis of citrate in N_2 , accompanying by a little of oxidation of C and H; second stage is violent combustion of C and H when the temperature is higher than $350^\circ C$.

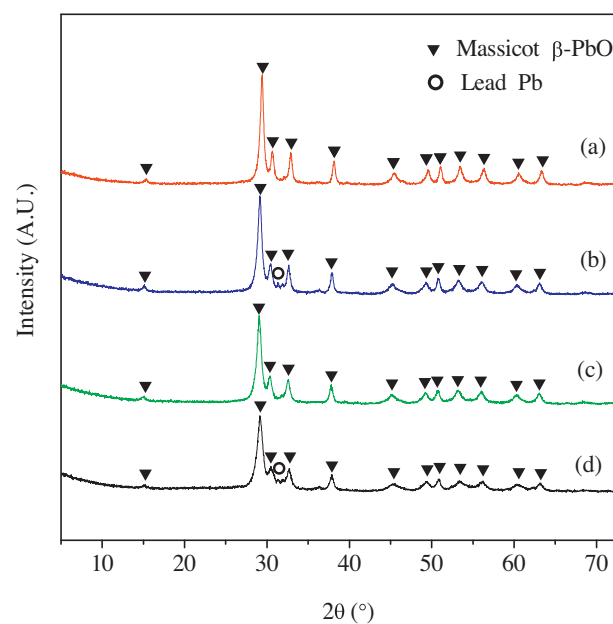


Fig. 7. XRD patterns of decomposition products from lead citrate at different temperature for 2 h in N_2 : (a) $295^\circ C$, (b) $335^\circ C$, (c) $350^\circ C$, and (d) $450^\circ C$.

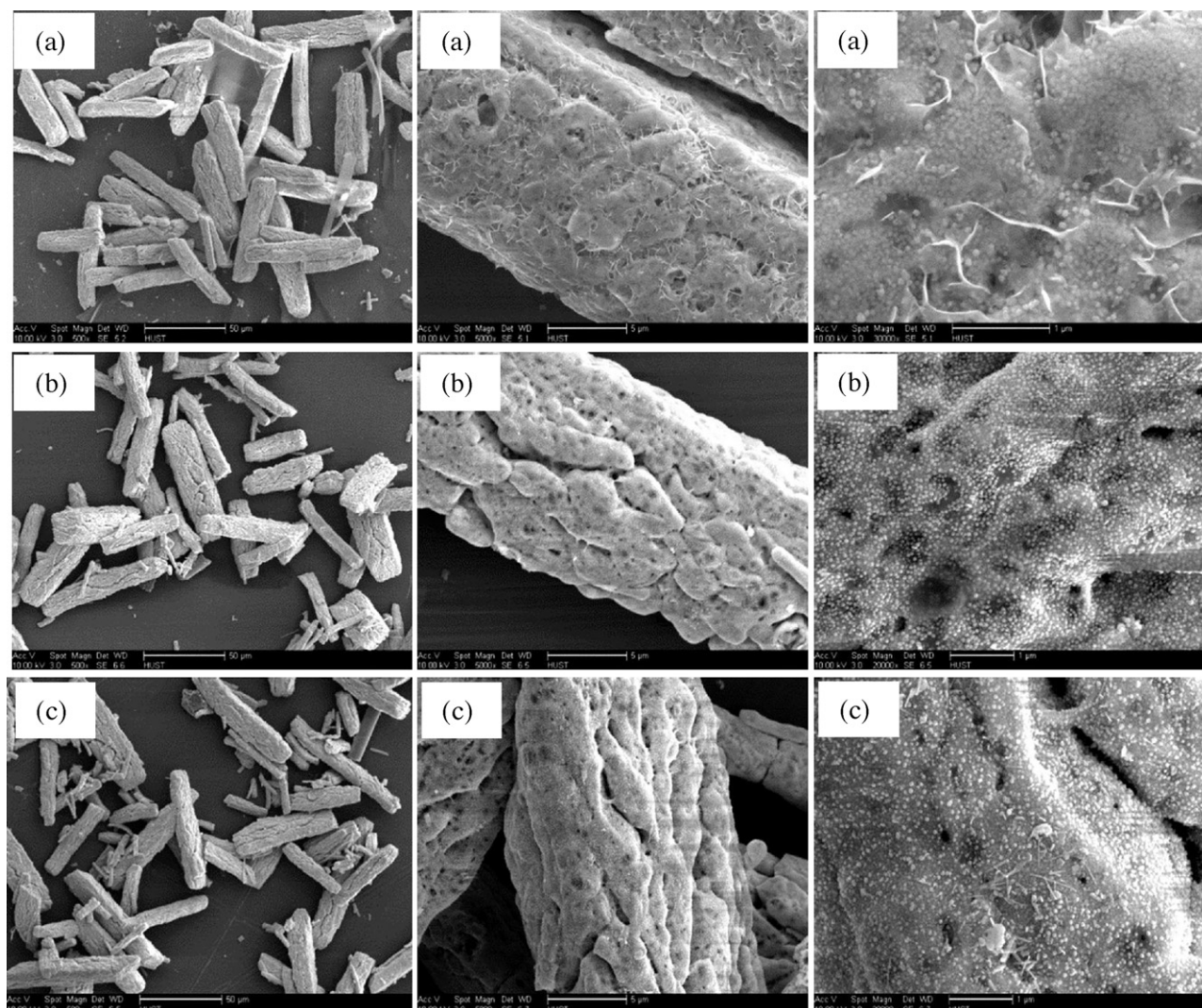


Fig. 8. SEM images of products decomposed at different temperatures in N_2 : (a) $295^\circ C$, (b) $350^\circ C$, and (c) $450^\circ C$.

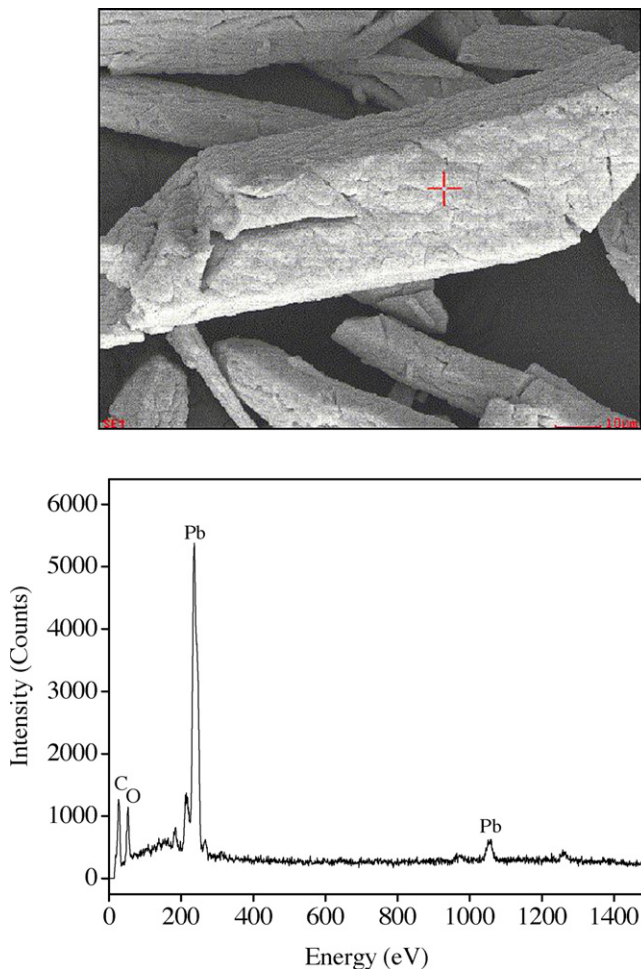


Fig. 9. EDX spectra of calcination product at 450 °C for 1 h in N₂.

3.3. Calcination in nitrogen gas

The samples of lead citrate were heated respectively in a tube furnace under nitrogen atmosphere at 295 °C, 335 °C, 350 °C, 400 °C and 450 °C for 2 h to investigate the thermal decomposition. The effect of the calcination temperature on weight loss of the citrate precursor is shown in Fig. 6. The weight loss increases with an increase in calcination temperature from 295 °C to 335 °C and it appears to be a plateau above 335 °C. The weight loss at 335 °C is 30 wt%.

The phase transformation of the calcination products shown in Fig. 7 was examined with X-ray diffraction technique. The XRD demonstrates that the crystalline contains massicot (β -PbO) and lead metal in temperature from 295 °C to 450 °C. The SEM images of products decomposed at different temperature are shown in Fig. 8. The products show similar morphology as the temperature increased. The EDX spectrum of product calcined at 450 °C is shown in Fig. 9. Some carbon is identified in calcination product by the EDX spectra. Therefore, the observed mass loss of 30% in nitrogen gas is about 7% less than the stoichiometric mass loss of 36.5% in the decomposition $Pb_3(C_6H_5O_7)_2 \cdot 3H_2O$ to PbO because of the formation of carbon in the decomposition products.

Brown [17] studied the thermal decomposition of lead citrate $Pb_3(C_6H_5O_7)_2 \cdot 2H_2O$ in N₂, and the results at temperature (305–325 °C) in his report showed that the pyrophoric metallic lead and carbon particles were produced. The presence of Pb can be reasoned from the reduction of PbO by carbon. However, in this

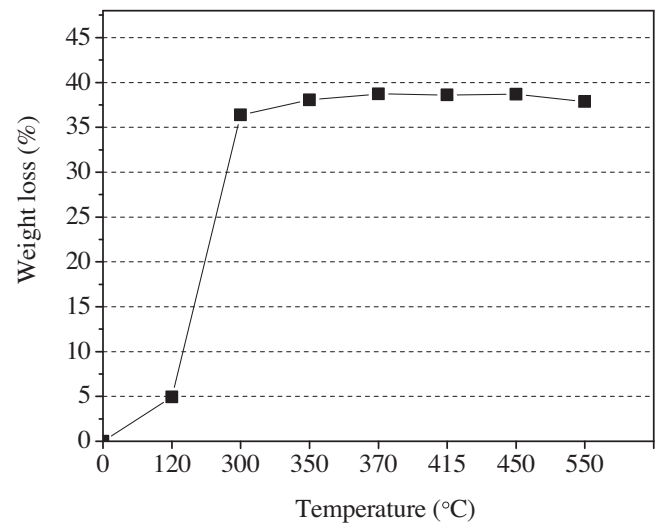


Fig. 10. Effects of calcination temperatures on weight loss after calcinations in air (1 h).

study, a mixture of PbO, Pb and C is obtained and CO₂ with H₂O are the main gas products during the thermal decomposition of $Pb_3(C_6H_5O_7)_2 \cdot 3H_2O$ in inert atmosphere.

3.4. Calcination in air

In air, lead citrate was calcined respectively for 1 h at 120 °C, 300 °C, 350 °C, 370 °C, 415 °C, 450 °C and 550 °C to remove all carbon and hydrogen. The effect of temperature on weight loss of the citrate precursor was investigated. Fig. 10 shows that the weight loss increases with an increase in temperature from 120 °C to 370 °C and then it keeps relatively stable at 38 wt% in the temperature range 370–450 °C. The weight loss of around 5% at

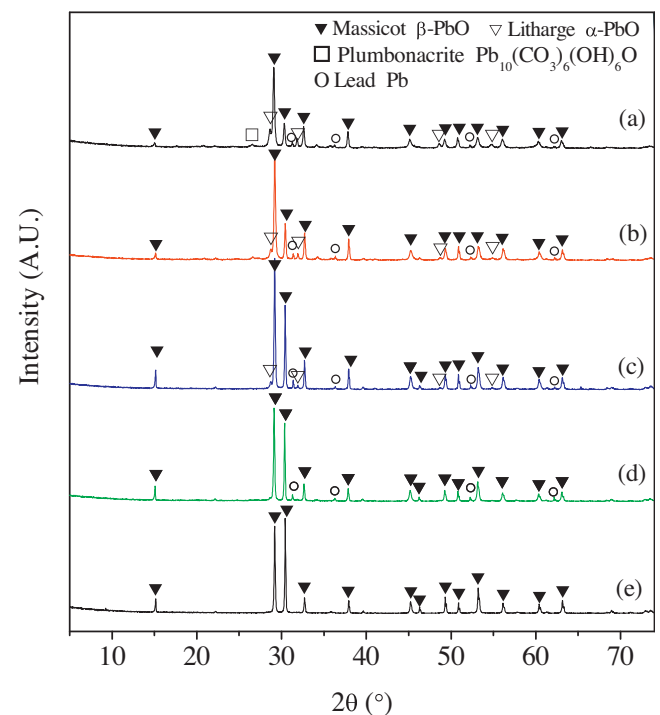


Fig. 11. XRD patterns of calcination-combustion products at different temperatures for 1 h in air: (a) 300 °C, (b) 350 °C, (c) 415 °C, (d) 450 °C, and (e) 550 °C.

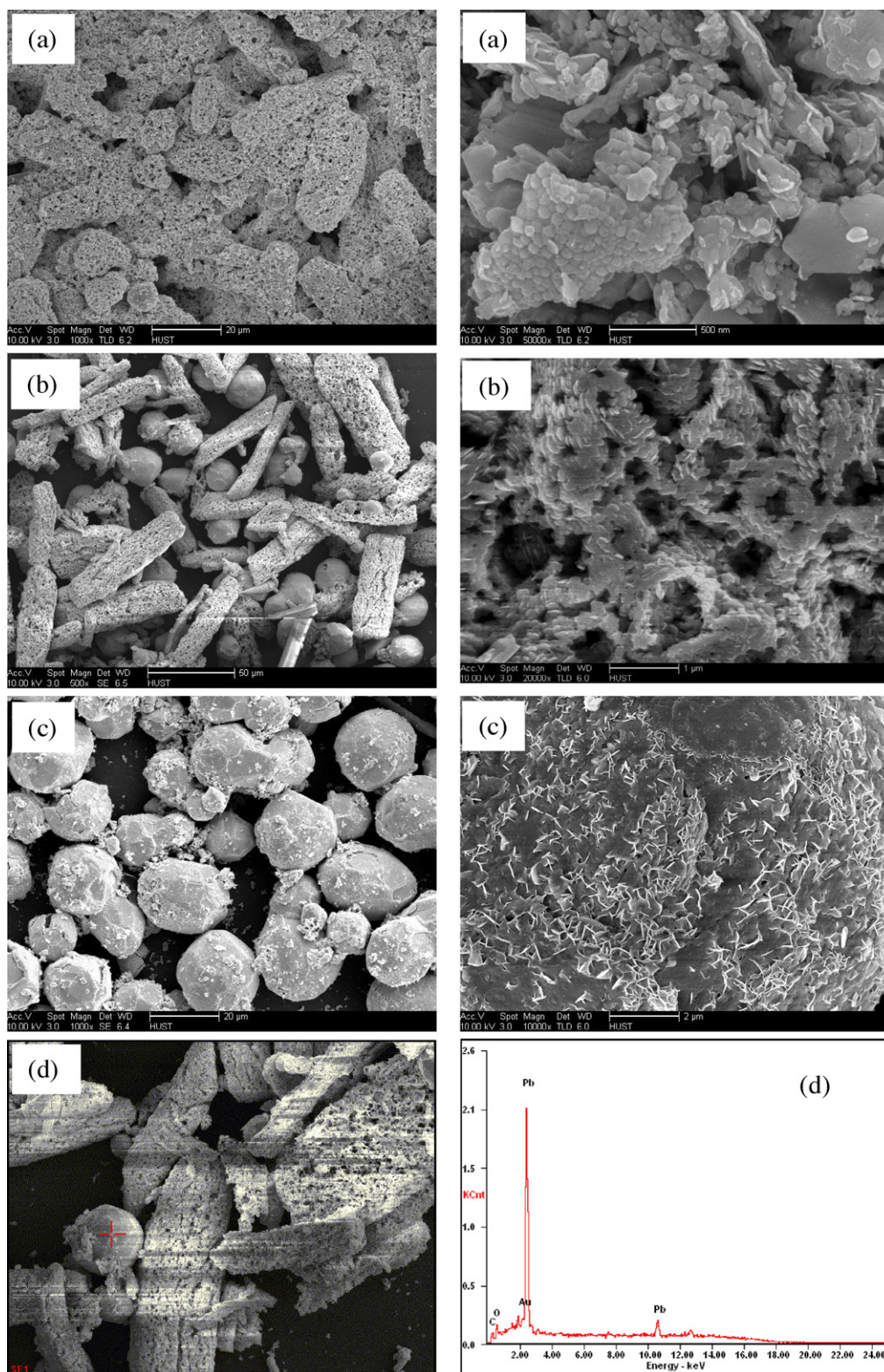


Fig. 12. SEM images of calcination–combustion products at different temperature for 1 h in air: (a) 300 °C, (b) 350 °C, and (c) 450 °C, and (d) EDX spectra of spherical substance in product at 350 °C.

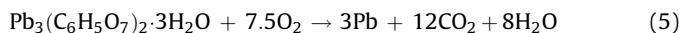
120 °C is consistent with the crystallization water content of lead citrate precursor ($\text{Pb}_3(\text{C}_6\text{H}_5\text{O}_7)_2 \cdot 3\text{H}_2\text{O}$). It is indicated that a dehydration reaction occurs in the temperature range of 120–300 °C.

If air supply is sufficient, PbO is the final product. According to the FTIR spectrums of tail gas (shown in Fig. 5(b)), CO_2 and H_2O are

the main components in the gas products. Therefore, the decomposition can be shown approximately as Eq. (4). The stoichiometric weight loss in Eq. (4) is 36.5%.



If the air is insufficient, Pb is the final product. The decomposition can be shown as Eq. (5). The stoichiometric weight loss in Eq. (5) is 41.0%.



The weight loss in the calcination experiments in air is around 38%, which is between 36.5% and 41.0%. It is indicated that the product is composed of PbO and Pb. The XRD patterns of products (Fig. 11) also demonstrate the composition of PbO and Pb.

Fig. 11 presents the XRD patterns of the calcination products in air at different temperature. The combustion products are β -PbO, α -PbO and metallic lead at 300 °C, 350 °C, 415 °C and 450 °C, with some intermediate phases which is $\text{Pb}_{10}(\text{CO}_3)_6(\text{OH})_6\text{O}$ at 300 °C. This results suggest that $\text{Pb}_3(\text{C}_6\text{H}_5\text{O}_7)_2 \cdot 3\text{H}_2\text{O}$ can be fully calcined in air at and above 350 °C. Additionally, the XRD patterns show that the diffraction peak for metallic Pb decreases as calcination temperature is increased.

Based on the results as mentioned above, it can be confirmed that there are two sequential stages taking place in the calcination of $\text{Pb}_3(\text{C}_6\text{H}_5\text{O}_7)_2 \cdot 3\text{H}_2\text{O}$ in air. When temperature is under 350 °C, lead citrate is decomposed and transformed into crystalline phases of β -PbO, α -PbO, Pb and small amount of intermediate containing C and H. The decomposition of this stage is alike of pyrolysis of lead citrate in N_2 . Compared with calcination products in N_2 (shown in Fig. 7), the difference is that metallic Pb are mostly oxidized to α -PbO in air. As temperature is higher than 350 °C, C and H in the intermediate combusted violently, accompanied with intense exothermic phenomenon and generation of CO_2 and H_2O . The temperature of 350 °C leads to producing β -PbO, α -PbO and a little of metallic Pb, and weight loss is 38 wt%. If temperature is higher than 488 °C, α -PbO will be transformed into β -PbO [18]. As it shown in Fig. 11(e), β -PbO is only crystal phase in the product.

Salavati-Niasari et al. [4] prepared PbO nanocrystals via decomposition of lead oxalate in air. He reported that a mixture of α -PbO and β -PbO nanocrystals was obtained at 235 °C, and the proportion of β -PbO increased as the temperature increased. Jia and Gao [19] synthesized single crystalline β -PbO nanorods through a hydrothermal processing of $\text{Na}_3\text{C}_6\text{H}_5\text{O}_7 \cdot 2\text{H}_2\text{O}$ and $\text{Pb}(\text{CH}_3\text{COO})_2 \cdot 3\text{H}_2\text{O}$. With lead citrate, formation of β -PbO rather than α -PbO was observed, in both air (by combustion) and N_2 (by decomposition). These results are consistent to the data in this paper.

The SEM images of the products from the citrate calcined at different temperatures are shown in Fig. 12. The results show that the morphology of products converts from porous columnar to spherical structure with increasing temperature. As shown in Fig. 12(a) at larger magnification, the products are agglomerated by ultrafine particles with the size of approximately in the range of 100–200 nm. When calcination temperature increases up to 350 °C and above, shown in Fig. 12(b), particulates agglomerate and grow larger. Furthermore, the morphology transforms from porous columnar into spherical structure at higher temperature as shown in Fig. 12(c). The spherical substance is also identified as the mixture of PbO and Pb by EDX spectra in Fig. 12(d). This indicates that the appearance of spherical structure could be attributed to the agglomeration and partial-melt of particles at higher calcination temperatures.

In order to determine the influence of calcination time, the citrate was calcined at 350 °C for 5–60 min in air respectively. The effect of calcination time on weight loss is shown in Fig. 13. The weight loss remains constant at 37.5 wt% for a calcination time of 15 min and more. This phenomenon suggests that the reactions during calcination–combustion are fast. The XRD patterns of combustion product at different calcination time are shown in Fig. 14. A small peak for intermediate which is organic lead

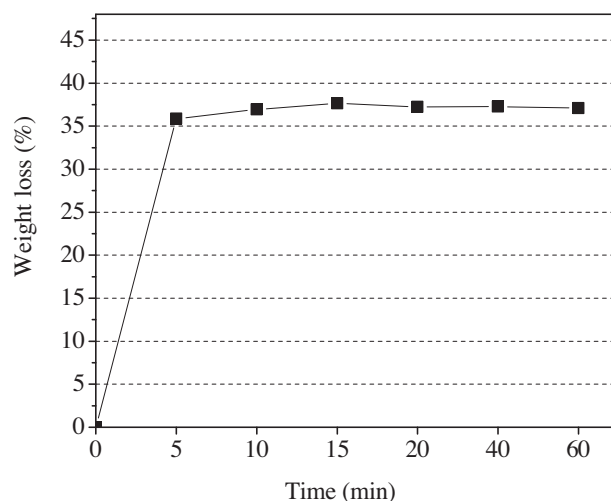


Fig. 13. Effects of the calcination time on weight loss in air at 350 °C.

compound $\text{Pb}_{10}(\text{CO}_3)_6(\text{OH})_6\text{O}$ can be seen at time of 15 min. However, the peak of the intermediate disappears after 20 min of calcination. Additionally, the XRD patterns show that the diffraction peak for metallic Pb decreases as calcination time is increased, that is, more metallic Pb is oxidized in air. This result suggests that the level of Pb oxidation can be adjusted by control of calcination atmosphere or oxidation potential to achieve a desirable PbO/Pb ratio.

By contrast with the $\text{Pb}(\text{C}_6\text{H}_6\text{O}_7) \cdot \text{H}_2\text{O}$, the $\text{Pb}_3(\text{C}_6\text{H}_5\text{O}_7)_2 \cdot 3\text{H}_2\text{O}$ is more economical and its crystal particle can grow up to the 5–50 μm length range. On the one hand, larger crystals can be filtrated easily. On the other hand, the mass transfer of oxygen becomes less efficient during the decomposition of big lead citrate particles. Thus, the calcination requires higher temperature in order to obtain pure products which contained only PbO and Pb, but high temperature will aggravate the agglomeration of the lead oxide products, which is resulting the decomposition temperature as a dilemma factor.

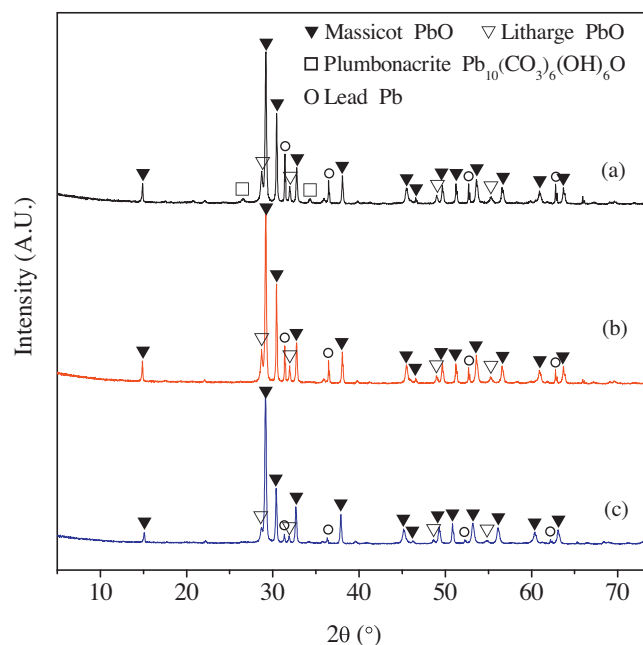


Fig. 14. XRD patterns of calcination–combustion products at 350 °C with different calcination times in air: (a) 15 min, (b) 20 min, and (c) 40 min.

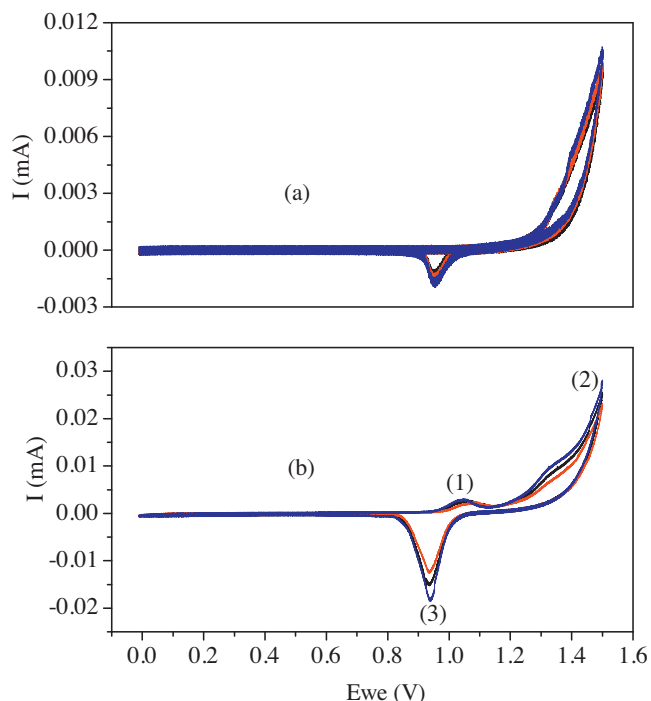
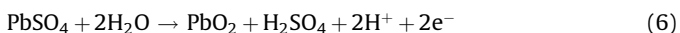


Fig. 15. Last three cyclic voltammograms of nanostructural lead oxide with 7 cycles of scanning. (a) The sample with porous columnar shape was synthesized at 350 °C for 1 h in air. (b) The sample with spherical structure was synthesized at 450 °C for 1 h in air.

3.5. Characterization of lead oxide with electrochemical technique–cyclic voltammetry

The lead oxide product with nano-size particulate will be used as anode material of lead acid battery. The properties of this kind of products were examined with electrochemical technique–cyclic voltammetry (CV) [20]. In the current research, the electrochemical technique was employed to determine the property of different nano-size lead oxide produced from the citrate precursor. Fig. 15 shows last three CV curves for 7 cycles of lead oxide. The lead oxides were synthesized at 350 °C and 450 °C respectively in air. They are of same crystal phase, but are different in microstructure (shown in Fig. 12). In the selected potential range from 0 V to +1.5 V, four peaks as marked numerically in Fig. 15(b) suggest some redox reactions possibly occurring in lead acid battery. The corresponding reactions are shown as described in Eqs. (6)–(8):



It is observed that when the scanning potential in anodic direction is around 1.1 V (vs. reference electrode), PbSO_4 is oxidized to PbO_2 as described in Eq. (6). At the same time under the high potential, evolution of oxygen from the aqueous system takes place, Eq. (7), and the possible residual PbSO_4 can be oxidized as well under such high potential. On the reverse scanning from potential 1.5 V, the reaction (8) occurs at about 0.95 V, that is, PbO_2 is reduced to PbSO_4 . The CV curves of nanostructural lead oxide with spherical structure have shown the spectrum of possible reactions occurring on anode in lead acid battery, but CV curves of

lead oxide with porous columnar shape are not integrity. It is indicated that microstructure of nanostructural lead oxide can influence on its electrochemical performance.

4. Conclusions

Preparation of nano-structural lead oxide has been investigated by decomposition of lead citrate in inert (nitrogen) and air atmospheres. The lead citrate ($\text{Pb}_3(\text{C}_6\text{H}_5\text{O}_7)_2 \cdot 3\text{H}_2\text{O}$), a precursor, was synthesized from spent lead acid battery pastes in citrate salt system. The citrate particle is in columnar shaped with length of 5–50 μm and diameter of 2–50 μm . If the calcination is carried out in nitrogen gas, the major decomposition products are orthorhombic phase β - PbO , metallic Pb and elemental C.

When the calcination–combustion is performed in air, lead citrate can be calcined completely at 350 °C for 20 min. The morphology of products converts from porous columnar to spherical structure with increasing temperature. Nano size product from calcination–combustion is achieved with particle size of around 100–200 nm. It is found to compose mainly of β - PbO with a small part of α - PbO and Pb. Both in air and N_2 decomposition, CO_2 and H_2O are the main gas products. The CV curves of nanostructural lead oxide with spherical structure show good reversible ability.

Acknowledgements

The authors would like to express thanks to the National Science Council of China (NSC 50804017) for the financial support and New Century Excellent Talents Project of Ministry of Education (NCET-09-0392). And the authors would like to appreciate financial supports of the Wuhan Planning Project of Science and Technology (20120321100) and the Key Program of Hubei Provincial Natural Science Foundation for Distinguished Young Scholars (2011CDA083). The authors would also like to extend the thanks to Analytical and Testing Center of Huazhong University of Science and Technology (HUST), which supplied the facilities for materials analysis.

References

- [1] A. Attar, M. Halali, M. Sobhani, R.T. Ghandehari, J. Alloys Compd. 509 (2011) 5825–5828.
- [2] C.H. Wu, F.S. Chen, S.H. Lin, C.H. Lu, J. Alloys Compd. 509 (2011) 5783–5788.
- [3] J. Wang, S. Zhong, G.X. Wang, D.H. Bradhurst, M. Ionescu, H.K. Liu, S.X. Dou, J. Alloys Compd. 327 (2001) 141–145.
- [4] M. Salavati-Niasari, F. Mohandes, F. Davar, Polyhedron 28 (2009) 2263–2267.
- [5] H. Sadeghzadeh, A. Morsali, V.T. Yilmaz, O. Buyukgungor, Mater. Lett. 64 (2010) 810–813.
- [6] M. Cruz, L. Hernan, J. Morales, L. Sanchez, J. Power Sources 108 (2002) 35–40.
- [7] H. Karami, M.A. Karimi, S. Haghdar, A. Sadeghi, R. Mir-Ghaserm, S. Mahdi-Khani, Mater. Chem. Phys. 108 (2008) 337–344.
- [8] H. Karami, M.A. Karimi, S. Haghdar, Mater. Res. Bull. 43 (2008) 3054–3065.
- [9] P.R. Arya, P. Jha, G.N. Subbanna, A.K. Ganguli, Mater. Res. Bull. 38 (2003) 617–628.
- [10] S. Verma, P.A. Joy, Mater. Res. Bull. 43 (2008) 3447–3456.
- [11] C.L. Mao, X.L. Dong, T. Zeng, Mater. Lett. 61 (2007) 1633–1636.
- [12] R.V. Kumar, V.P. Kotzeva, S. Sonmez, Lead recycling, World Intellectual Property Organization, WO2008056125-A1, 2008, p. 1–35.
- [13] J.K. Yang, R.V. Kumar, D.P. Singh, J. Chem. Technol. Biotechnol. 87 (2012) 1480–1488.
- [14] J.K. Yang, X.F. Zhu, R.V. Kumar, Mater. Chem. Phys. 131 (2011) 336–342.
- [15] L. Li, X.F. Zhu, D.N. Yang, L.X. Gao, J.W. Liu, R.V. Kumar, J.K. Yang, J. Hazard. Mater. 203–204 (2012) 274–282.
- [16] R.R. Hao, X.Y. Fang, S.C. Niu, The Series of Inorganic Chemistry (Third Volume), China Science Press, Beijing, 1988.
- [17] M.E. Brown, J. Chem. Soc., Faraday Trans. 1: Phys. Chem. Condens. Phases 69 (1973) 1202–1212.
- [18] M.J. Munson, R.E. Riman, J. Therm. Anal. Calorim. 37 (1991) 2555–2566.
- [19] B.P. Jia, L.A. Gao, Mater. Chem. Phys. 100 (2006) 351–354.
- [20] W. Visscher, J. Power Sources 1 (1977) 257–266.